Supporting Information

Separator pore size induced oriented Zn deposition

Kesong Yu[a], Yuehua Wen[a], Mengyu Yan[a,d]*, Xuan Teng[a], Wei Yang[a], Sitian Lian[a], Jianyong Zhang[a], Farao Zhang[b], Xiaoyu Jiang[b]*, Yanzhu Luo[c]*, Liqiang Mai[a,d]*

a. State Key Laboratory of Advanced Technology for Materials Synthesis and Processing, School of Materials Science and Engineering, International School of Materials Science and Engineering, Wuhan University of Technology, Wuhan 430070, China.

b. Ningbo MaterChem Technology Co. Ltd, Ningbo 315830, China.

c. College of Chemistry, Huazhong Agricultural University, Wuhan 430070, China.

d. Hubei Longzhong Laboratory, Wuhan University of Technology (Xiangyang Demonstration Zone), Xiangyang 441000, China.

*Correspondence to: ymy@whut.edu.cn; mlq518@whut.edu.cn; xiaoyuj1991@outlook.com; luoyanzhu@mail.hzau.edu.cn.

Experimental Section

Separator preparation: The commercial polyethylene (PE) separator (Intelligent Materials Pvt. Ltd., USA, 9μm or 16 μm) was passed through the plasma zone at a speed of 100 mm/min in a roll-to-roll way, corresponding to an active time of 1 min. The plasma was ignited at a voltage power of 30 W through two plate electrodes with a flow rate of air of 200 mL/min at 10 Pa. The plasma-treated PE separator was then passed through an isopropanol solution containing 0.12 mol/L of titanium isopropoxide (Aladdin), 0.28 mol/L of deionized water, and 0.03 mol/L of HCl at 70 °C in a roll-to-roll way. The reaction time for each separator is approximately 2 h. After rinsing with water and drying at 70 °C, we obtained the TiO_2-grafted PE separator.

Synthesis method of VO_2: Mix 0.5 g oxalic acid dihydrate, 0.36 g V_2O_5, and 40ml deionized water in a reaction flask. Stir the mixture using a magnetic stirrer at room temperature for 4 hours. Subsequently, allow the reaction to proceed at 180°C for 24 hours. Wash the resulting product several times, dry it, and obtain a deep blue powder.

Materials Characterization: Scanning electron microscopy (SEM) images were collected on a JEOL-7100F microscope at 20 kV. X-ray photoelectron spectroscopy (XPS) was carried out on a SHIMADZU (Kratos) Axis Supra equipped with an Al Ka monochromated X-ray source. The contact angle was measured by the KRÜSS DSA100 Drop Shape Analyzer. X-ray diffraction (XRD) was performed by Bruker D8 and EVASTAR Y2 X-ray diffractometer with a Cu Kα X-ray source (λ = 1.5418 Å). Pole figures data for zinc metal were collected in a field emission gun SEM (JSM-IT800) equipped with an EBSD system. EBSD was performed at 10 kV at a 70° inclination using the Oxford Instruments detector.

Electrochemical measurements: The Zn||Zn symmetric coin cells are assembled, in which the Zn plates serve as both positive and negative electrodes, 1 M $ZnSO_4$ as the electrolyte. The Celgard 3501, GF/A, and TiO_2-PE (16 μm) are selected as separator in the coin cells. The charge and discharge were performed at a current density of 1 mA cm^{-2} and an areal capacity of 1 mAh cm^{-2} (NEWARE battery testing system). The Zn||VO_2 cells used in the experiments were 2032-coin models, with GF/A filters or TiO_2-PE (9 μm) separator and 2 M $ZnSO_4$ aqueous electrolyte. VO_2 cathode films were prepared by compressing a mixture of active materials: Super P: polytetrafluoroethylene (PTFE) in a mass ratio of 7:2:1, then they are punched into circular shapes with 10 mm, utilizing Ti foil as the current collector. The mass loading of the VO_2 electrode is about 1 mg cm^{-2}. The Zn||VO_2 batteries were discharged to 0.2 V and charged to 1.2 V at constant current density. Galvanostatic charge-discharge measurements were performed with battery testing system (LAND CT2001A). The CA and CV measurements were performed on an electrochemical workstation (CHI760E).

***In situ* XRD measurements**: A lab-made *in situ* cell mold was utilized for this study. The cathode electrode was made of a Be window with a ~100 nm Titanium metal layer, with Zn foil as the anode electrode and the 1M $ZnSO_4$ as the electrolyte. TiO_2-PE and GF/A served as separators, respectively. The *in situ* cell was discharged at a current density of 1 mA cm^{-2} for 1 hour, subsequently charged until approaching the 0.5 V cutoff potential, and then cycled. The *in situ* XRD data was collected simultaneously every 2 mins.

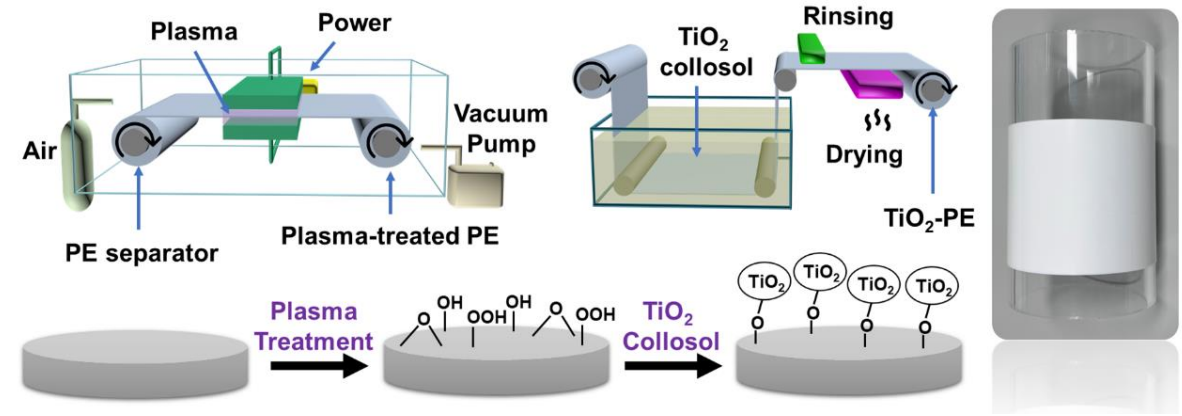

Scheme 1. Schematic illustration for the TiO_2-grafted PE (TiO_2-PE) separator preparation

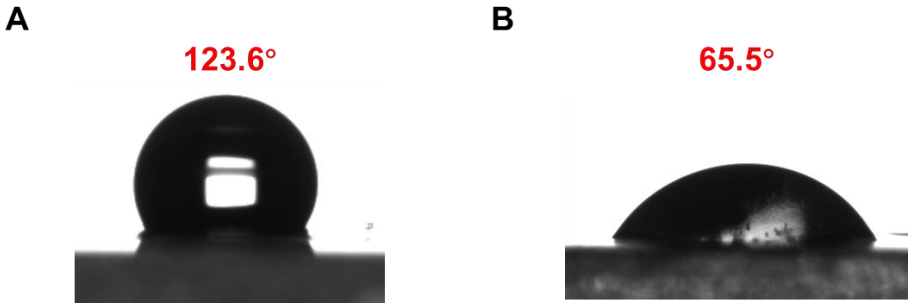

Figure S1 Contact angle test photos of PE (**A**) and TiO_2-PE (**B**) separators

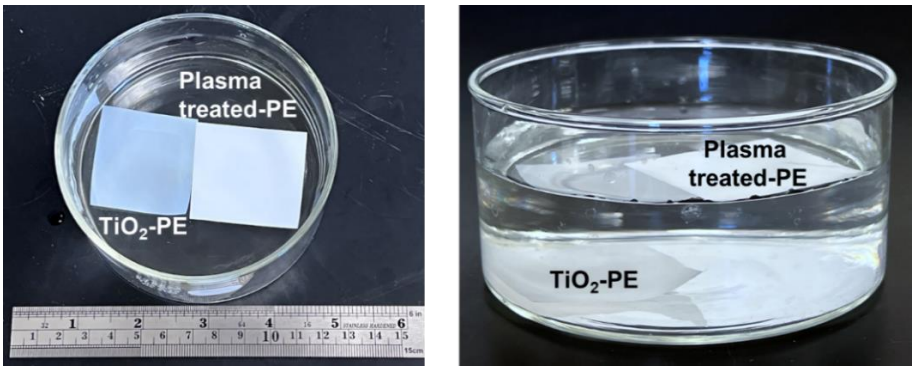

Figure S2 Photographs of the TiO_2-PE and plasma-treated PE separator immersed in deionized water

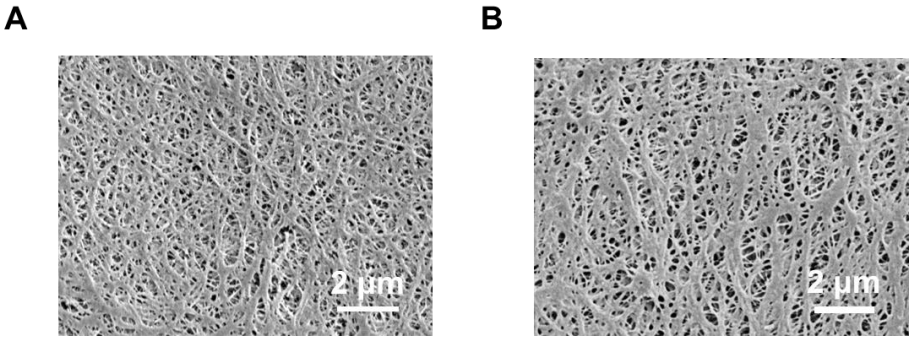

Figure S3 The SEM images of PE (**A**) and TiO_2-PE (**B**) separators

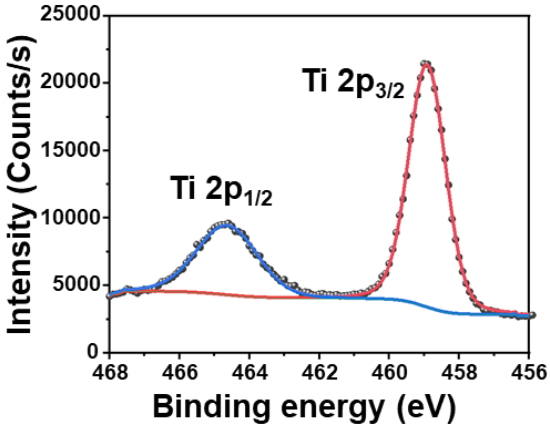

Figure S4 XPS peak of Ti 2p of the TiO_2-PE separator.

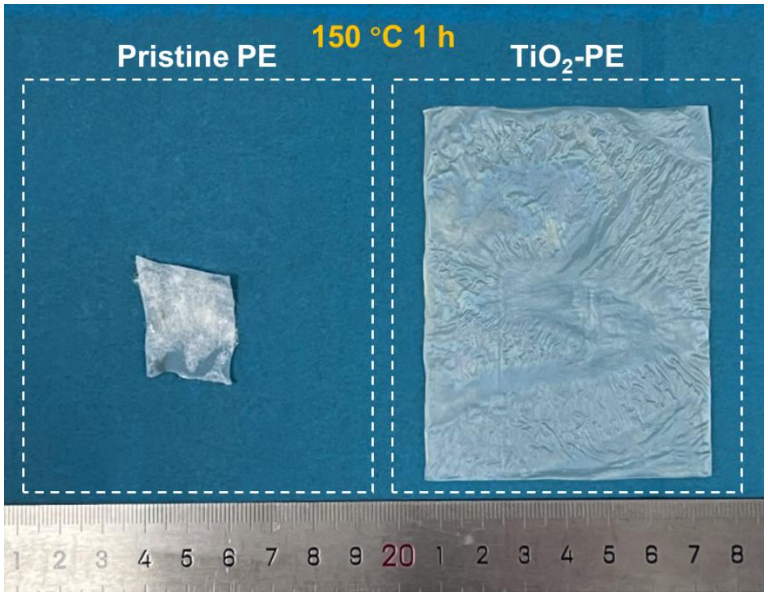

Figure S5 Photographs of the pristine and TiO_2-PE separator after storage at 150 °C for 1h. The white dashed square shows the original size of the separators.

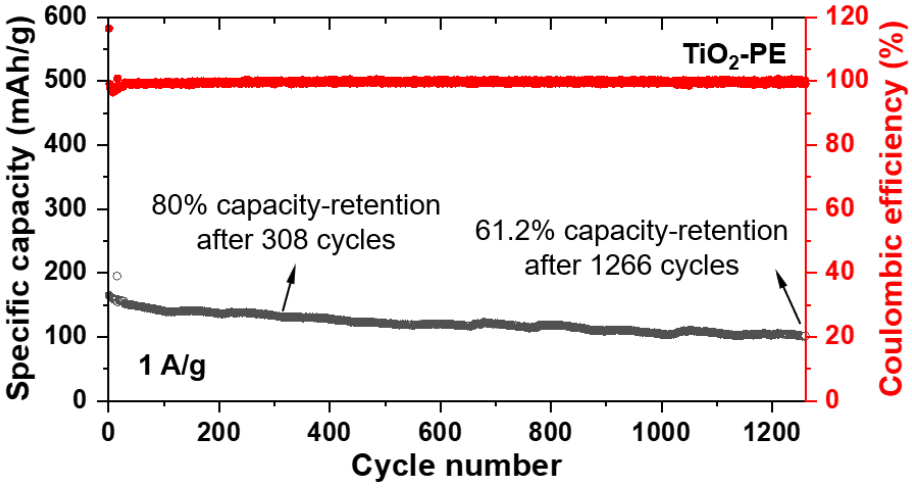

Figure S6. Cycling performance for Zn||VO_2 full cells with the TiO_2-PE separator at 1 A g^{-1}.

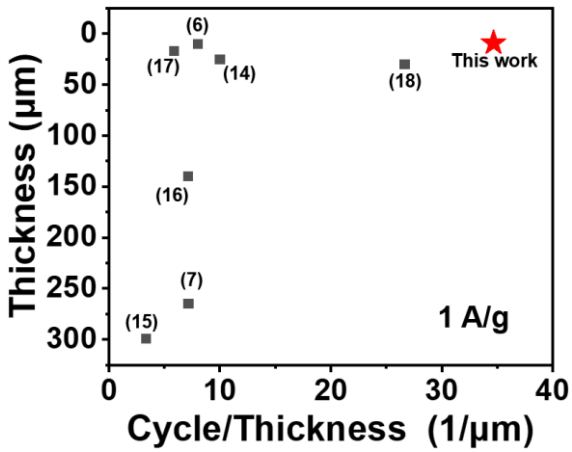

Figure S7. A diagram of the relationship between the cycle number and separators' thickness (Data from Table S3).

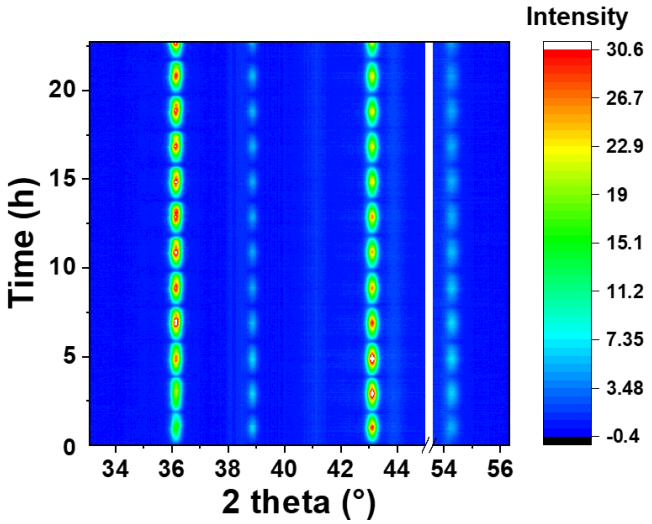

Figure S8 In-situ XRD patterns of deposited Zn with TiO_2-PE

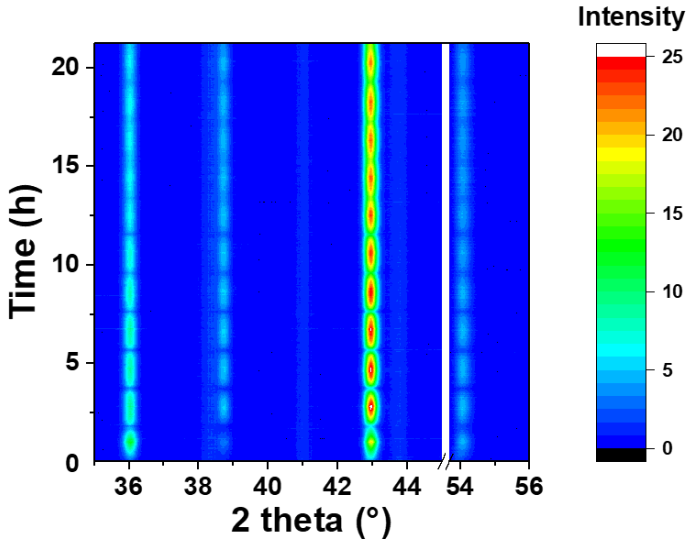

Figure S9 In-situ XRD patterns of deposited Zn with GF/A

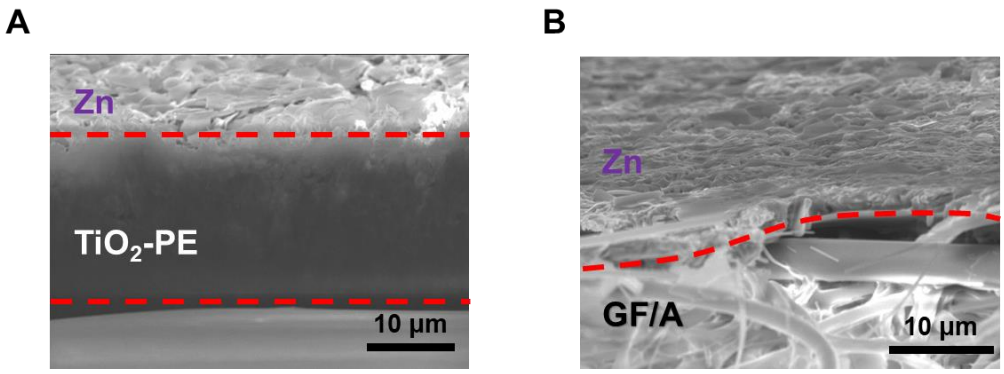

Figure S10 Side-view SEM images of Zn deposited on TiO_2-PE (**A**) and GF/A separators (**B**).

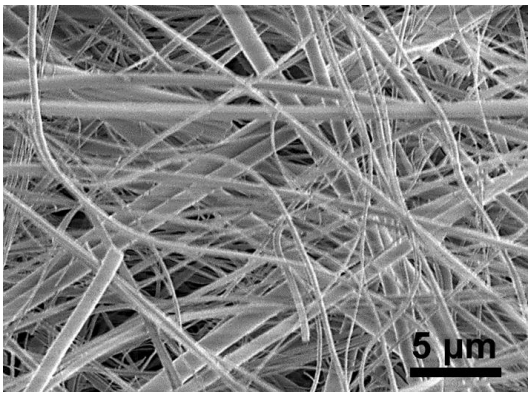

Figure S11 The SEM images of GF/A separators.

Table S1 The data of Figure 1. Dependence of separator thickness on Zn ion battery energy density. (mainly based on the commercialized separators). The energy density is calculated based on the mass of the cathode, anode, and electrolyte-soaked separator. In our calculation model, we set cathode mass and anode mass to 15 and 10 milligrams, respectively. Our calculation formula is as follows:
Corrected energy density = Capacity × Operating voltage × Cathode mass / (Cathode mass + Anode mass + Separator with electrolyte mass)

Number	Separator materials	Thickness (μm)	Capacity (mAh/g)	Operating voltage (V)	Energy density (Wh/kg)	Separator with electrolyte mass (mg)	Corrected energy density (Wh/kg)
1	Glass fiber[1]	**675**	285	1.44	410.4	292.50	**19.39**
2	Glass fiber[2]	**675**	381	1	381	292.50	**18.00**
3	Celgard 3501[3]	**25**	150	1	150	7.32	**69.62**
4	Glass fiber (GF/C)[4]	**260**	394	1	394	83.85	**54.29**
5	Biomass nanofibers[5]	**7**	173.8	1.3	225.94	2.05	**125.29**
6	Bamboo cellulose[6]	**10**	175	1.3	227.5	2.93	**122.19**
7	Glass fiber[7]	**265**	180	1.4	252	85.46	**34.22**
8	Glass fiber (GF/D)[8]	**675**	374	1.3	486.2	292.50	**22.97**
9	Glass fiber (GF/A)[9]	**260**	218	1.3	283.4	83.85	**39.05**

Table S2 The data of Figure 2e. Some separator materials for zinc ion batteries, including their thickness (unit: μm), cycle number of full cell (Current density: 0.2~0.5 A/g) and cycle per thickness. (The recording principle of cycle number is that the capacity retention rate is greater than 80%)

Number	Separator materials	Current density (A/g)	Thickness (μm)	Cycle	Cycle/thickness
3	Celgard 3501[3]	0.2	**25**	300	**12**
10	-SO_3H mask PP separator[10]	0.2	**140**	200	**1.43**
5	Biomass nanofibers[5]	0.3	**7**	100	**14.29**
11	Sn-coated separator[11]	0.3	**30**	600	**20**
12	PVDF-Li separator[12]	0.5	**20**	475	**23.75**
13	SPSF@PMIA[13]	0.5	**80**	1000	**12.5**
	TiO_2-PE (This work)	0.25	**9**	256	**28.44**

Table S3 The data of Figure S7. Some separator materials for zinc ion batteries, including their thickness (unit: μm), cycle number of full cell (Current density: 1 A/g) and cycle per thickness. (The recording principle of cycle number is that the capacity retention rate is greater than 80%)

Number	Separator materials	Current density (A/g)	Thickness (μm)	Cycle	Cycle/thickness
6	Bamboo cellulose[6]	1	**10**	80	**8**
7	Glass fiber[7]	1	**265**	1900	**7.17**
14	Zn-Nafion separator[14]	1	**25**	250	**10**
15	GF/PBPT[15]	1	**299**	1000	**3.34**
16	Cotton cellulose Separator[16]	1	**140**	1000	**7.14**
17	Polypyrene cellulose paper[17]	1	**17**	100	**5.88**
18	Graphene oxide cellulose separator[18]	1	**30**	800	**26.67**
	TiO_2-PE (This work)	1	**9**	308	**34.22**

References:

[1] H. Pan, Y. Shao, P. Yan, Y. Cheng, K. S. Han, Z. Nie, C. Wang, J. Yang, X. Li, P. Bhattacharya, K. T. Mueller, J. Liu, Reversible aqueous zinc/manganese oxide energy storage from conversion reactions, Nat. Energy 1(5) (2016) 16039, https://doi.org/10.1038/nenergy.2016.39.

[2] M. Yan, P. He, Y. Chen, S. Wang, Q. Wei, K. Zhao, X. Xu, Q. An, Y. Shuang, Y. Shao, K. T. Mueller, L. Mai, J. Liu, J. Yang, Water-lubricated intercalation in $V_2O_5{\cdot}nH_2O$ for high-capacity and high-rate aqueous rechargeable zinc batteries, Adv.

Mater. 30(1) (2018) 1703725, https://doi.org/10.1002/adma.201703725.

[3] C. Xia, J. Guo, Y. Lei, H. Liang, C. Zhao, H. N. Alshareef, Rechargeable aqueous zinc-ion battery based on porous framework zinc pyrovanadate intercalation cathode, Adv. Mater. 30(5) (2018) 1705580, https://doi.org/10.1002/adma.201705580.

[4] Q. Pang, C. Sun, Y. Yu, K. Zhao, Z. Zhang, P. M. Voyles, G. Chen, Y. Wei, X. Wang, $H_2V_3O_8$ nanowire/graphene electrodes for aqueous rechargeable zinc ion batteries with high rate capability and large capacity, Adv. Energy Mater. 8(19) (2018) 1800144, https://doi.org/10.1002/aenm.201800144.

[5] Y. Zhang, X. Li, L. Fan, Y. Shuai, N. Zhang, Ultrathin and super-tough membrane for anti-dendrite separator in aqueous zinc-ion batteries, Cell Reports Phys. Sci. 3(4) (2022), https://doi.org/10.1016/j.xcrp.2022.100824.

[6] J. Fu, H. Wang, P. Xiao, C. Zeng, Q. Sun, H. Li, A high strength, anti-corrosion and sustainable separator for aqueous zinc-based battery by natural bamboo cellulose - ScienceDirect, Energy Storage Mater. 48 (2022) 191-191, https://doi.org/10.1016/j.ensm.2022.02.052.

[7] Y. Lin, Y. Hu, S. Zhang, Z. Xu, T. Feng, H. Zhou, M. Wu, Highly reversible aqueous zinc-ion battery using the chelating agent triethanolamine as an electrolyte additive, CrystEngComm 24(45) (2022) 7950-7961, http://dx.doi.org/10.1039/D2CE01089E.

[8] X. Zhang, J. Li, K. Qi, Y. Yang, D. Liu, T. Wang, S. Liang, B. Lu, Y. Zhu, J. Zhou, An ion-sieving janus separator toward planar electrodeposition for deeply rechargeable Zn-metal anodes, Adv. Mater. 34(38) (2022) 2205175, https://doi.org/10.1002/adma.202205175.

[9] K. Han, F. An, F. Yan, H. Chen, Q. Wan, Y. Liu, P. Li, X. Qu, High-performance aqueous Zn–MnO_2 batteries enabled by the coupling engineering of K^+ pre-intercalation and oxygen defects, J. Mater. Chem. A 9(28) (2021) 15637-15647, http://dx.doi.org/10.1039/D1TA03994F.

[10] S. Kim, X. Yang, K. Yang, H. Guo, M. Cho, Y. J. Kim, Y. Lee, Recycling respirator masks to a high-value product: From COVID-19 prevention to highly efficient battery separator, Chem. Eng. J. 430 (2022), https://doi.org/10.1016/j.cej.2021.132723.

[11] Z. Hou, Y. Gao, H. Tan, B. Zhang, Realizing high-power and high-capacity zinc/sodium metal anodes through interfacial chemistry regulation, Nat. Commun. 12(1) (2021), https://doi.org/10.1038/s41467-021-23352-0.

[12] F. Zhang, F. Huang, R. Huang, N. Dong, S. Jiao, R. Cao, H. Pan, Hierarchical porous separator with excellent isotropic modulus enabling homogeneous Zn^{2+} flux for stable aqueous Zn battery, Science China-Materials 66(3) (2023) 982-991, https://doi.org/10.1007/s40843-022-2239-8.

[13] W. Hu, J. Ju, Y. Zhang, W. Tan, N. Deng, W. Liu, W. Kang, B. Cheng, Deposition behavior regulated by an SPSF@PMIA nanofiber separator for high-performance zinc ion batteries, J. Mater. Chem. A 10(46) (2022) 24761-24771, http://dx.doi.org/10.1039/D2TA06830C.

[14] B. Wu, Y. Wu, Z. Lu, J. Zhang, N. Han, Y. Wang, X.-m. Li, M. Lin, L. Zeng, A cation selective separator induced cathode protective layer and regulated zinc deposition for zinc ion batteries, J. Mater. Chem. A 9(8) (2021) 4734-4743, http://dx.doi.org/10.1039/D0TA11841A.

[15] X. Liu, W. Wei, Y. Yang, Y. Li, Y. Li, S. Xu, Y. Dong, R. He, A porous membrane electrolyte enabled by poly(biphenyl piperidinium triphenylmethane) for dendrite-free zinc anode with enhanced cycling life, Chem. Eng. J. 437 (2022) 135409, https://doi.org/10.1016/j.cej.2022.135409.

[16] W. Zhou, M. Chen, Q. Tian, J. Chen, X. Xu, C.-P. Wong, Cotton-derived cellulose film as a dendrite-inhibiting separator to stabilize the zinc metal anode of aqueous zinc ion batteries, Energy Storage Mater. 44 (2022) 57-65, https://doi.org/10.1016/j.ensm.2021.10.002.

[17] C. Peng, Y. Zhang, S. Yang, L.-L. Zhang, Z. Wang, Flexible zincophilic polypyrrole paper interlayers for stable Zn metal anodes: Higher surface flatness promises better reversibility, Nano Energy 98 (2022) 107329, https://doi.org/10.1016/j.nanoen.2022.107329.

[18] J. Cao, D. Zhang, C. Gu, X. Wang, S. Wang, X. Zhang, J. Qin, Z.-S. Wu, Manipulating crystallographic orientation of zinc deposition for dendrite-free zinc ion batteries, Adv. Energy Mater. 11(29) (2021) 2101299, https://doi.org/10.1002/aenm.202101299.